Effect of anharmonicity on the hcp to bcc transition in beryllium at high-pressure and high-temperature conditions

Jia-Wei Xian,[1] Jun Yan,[1] Hai-Feng Liu,[1] Tao Sun,[2] Gong-Mu Zhang,[1] Xing-Yu Gao,[1,3] and Hai-Feng Song[1,3,*]

[1]*Institute of Applied Physics and Computational Mathematics, Beijing 100094, China*

[2]*Key Laboratory of Computational Geodynamics, University of Chinese Academy of Sciences, Beijing 100049, China*

[3]*CAEP Software Center for High Performance Numerical Simulation, Beijing 100088, China*

(Received 19 November 2018; revised manuscript received 7 January 2019; published 6 February 2019)

We investigate the hcp to bcc phase transition in beryllium (Be) at high-pressure and -temperature (PT) conditions. A recently developed hybrid approach that combines first-principles molecular dynamics and lattice dynamics is used to account for anharmonic contributions to the free energy. Anharmonic effects are shown to be strong at high T in both hcp and bcc Be. They are stronger in hcp Be than in bcc Be, as evidenced by the larger anharmonic vibrational entropy of hcp Be. We find that anharmonicity has a significant influence on the hcp to bcc transition at high-PT conditions. It substantially enlarges the stability domain of hcp Be at high T compared with that calculated under the quasiharmonic approximation (QHA), as a result bringing theoretical predictions into good consistency with recent experimental observations. After considering anharmonic effects, the calculated pressure and temperature of the hcp/bcc/liquid triple point increase from about 85 to 165 GPa, and from about 3300 to 4200 K, respectively, and the predicted Clapeyron slope at the triple point takes a value of -7.4 ± 0.7 K/GPa, noticeably larger in magnitude than previous QHA results in the range of -3 to 2 K/GPa.

DOI: 10.1103/PhysRevB.99.064102

I. INTRODUCTION

Although beryllium (Be) has a simple electronic structure with only four electrons, it possesses unique properties that distinguish itself from all other metals. For example, at ambient conditions beryllium is the metal with the lowest c/a ratio (1.568) of the hexagonal close-packed (hcp) phase, the lowest Poisson's ratio (0.05), and the highest Debye temperature (1471 K) [1,2]. The rich physical properties of beryllium have enabled a broad range of technological applications in areas such as aeronautics, communications, and nuclear power industry. A lot of recent attention has been paid to the potential application as an ablator material for fuel capsule in inertial confinement fusion, where in these experiments beryllium can subject to pressure and temperature on the order of $P \sim 200$ GPa and $T \sim 4000$ K, respectively [3–5].

Beryllium has the hcp structure at ambient conditions. As temperature rises, the hcp phase was found to transform into the body-centered-cubic (bcc) phase at $T = 1523$ K, just before melting at $T_m = 1551$ K [6]. The hcp/bcc phase line has been observed up to a few GPa, with inconsistent values reported for the Clapeyron slope, a negative value of -52 ± 8 K/GPa for $0 < P < 6$ GPa by Francois and Contre [7], and a positive value of 43 ± 7 K/GPa for $0 < P < 0.6$ GPa by Abey [8]. According to the phase diagram, hcp to bcc transition should also occur at much higher pressures. Considerable efforts have been made to locate this high-pressure transition. In a recent static diamond-anvil-cell (DAC) experiment, Lazicki *et al.* explored in a wide PT range, but detected no sign of the bcc phase up to $P = 205$ GPa and $T = 4000$ K [9]. In addition, the bcc phase was never observed in other static experiments at ambient temperature up to 200 GPa [10–14]. First-principles calculations predicted a large span of values for the transition pressure at $T = 0$ K, from about 180 to 420 GPa [15–23]. Among these results, the most recent ones are highly consistent with each other, all pointing to a value between 380 and 390 GPa [20–23]. The full hcp/bcc phase line as a function of P and T at high pressures has been obtained by three calculations based on the quasiharmonic approximation (QHA) [19–21]. At $T > 3300$ K, the stability domains of the hcp phase obtained by two latest QHA calculations [20,21] are too small compared with those observed in the static experiment of Lazicki *et al.* [9]. The earlier QHA calculation of Benedict *et al.* [19] predicted significantly larger hcp/bcc transition pressures at high T. This originates from the large value obtained at $T = 0$ K, about 420 GPa, which is apparently larger than that given by the other two QHA calculations, about 390 GPa. Despite that the calculated transition pressures can be very different, the variation tendency of the transition pressure with temperature, or equivalently the Clapeyron slope, is very similar in all three QHA calculations. The values of the Clapeyron slope at the hcp/bcc/liquid triple point predicted by three QHA calculations are all close to zero, lying in the range of -3 to 2 K/GPa [19–21].

To help resolve the controversies on the hcp/bcc transition in beryllium, it is important to go beyond QHA and consider anharmonicity in theoretical calculations. Anharmonicity is not only crucial for the high-temperature stabilization of crystal structures that are dynamically unstable at zero temperature, e.g., bcc Be [20], but may also contribute

*song_haifeng@iapcm.ac.cn

significantly to the free energy and thus has a great influence on the high-temperature phase boundary. There has been much recent progress in the theoretical treatment of anharmonic effects. Several effective computational methods were developed, such as self-consistent *ab initio* lattice dynamics (SCAILD) [24,25], self-consistent harmonic approximation (SCHA) [26,27], and temperature-dependent effective potential (TDEP) [28,29]. These include a vibrational normal mode analysis method developed by Zhang *et al.* [30,31], which is a hybrid approach that combines first-principles molecular dynamics (MD) and lattice dynamics (LD). In this method, anharmonic phonon frequencies and the corresponding phonon lifetimes can be obtained accurately at the same time. The resulting frequencies can be used to compute the free energy with anharmonic contributions [30–32], while the associated lifetimes can be used in thermal conductivity calculations [33–35].

Using vibrational normal mode analysis to account for anharmonic effects, Lu *et al.* recently resolved the dynamic stability of bcc Be at low-P–high-T conditions, and obtained an hcp/bcc phase boundary close to the melting line up to $P = 11$ GPa [32]. The predicted Clapeyron slope has a positive value of 41 ± 4 K/GPa, in good agreement with Abey's measurement of 43 ± 7 K/GPa [8]. Considering that anharmonicity becomes stronger as temperature rises, and that the hcp/bcc transition temperature at high pressures (e.g., at $P > 100$ GPa) can be much larger than that at low pressures (e.g., at $P < 10$ GPa) [9,19–21], anharmonic effects should continue to play an important role on the hcp/bcc transition in beryllium at high-PT conditions. However, to date an explicit treatment of anharmonic effects at these conditions is still missing.

To fill this gap, in this work we investigate the hcp/bcc transition in beryllium at high-PT conditions, where vibrational normal mode analysis [30,31] is performed to account for anharmonic contributions to the free energy of hcp and bcc Be. We show that at high T anharmonic effects are strong in both hcp and bcc Be. They are more pronounced in hcp Be than in bcc Be, as manifested by the larger anharmonic vibrational entropy of hcp Be. We find that anharmonicity significantly influences the hcp/bcc transition in beryllium at high-PT conditions. The consideration of it substantially enlarges the calculated stability domain of hcp Be at high T, leading to good agreement with experimental observations. As a result of anharmonic effects, the calculated pressure and temperature of the hcp/bcc/liquid triple point increase from about 85 to 165 GPa, and from about 3300 to 4200 K, respectively, and the predicted Clapeyron slope at the triple point of -7.4 ± 0.7 K/GPa is observably larger in magnitude than previous QHA values in the range of -3 to 2 K/GPa.

This paper is organized as follows: Section II outlines the basic theories of QHA and vibrational normal mode analysis; the computational details are summarized in Sec. III; Sec. IV contains our computed results, where anharmonic effects on the vibrational properties of hcp and bcc Be, and on the hcp/bcc phase transition at high-PT conditions, are elaborated, and an important technical detail concerning the convergence of free energy and phase boundary with respect to k-mesh sampling is discussed; Sec. V concludes this paper.

II. THEORY

A standard method for the theoretical determination of phase boundary is to conduct free-energy comparison. The central task is to compute the Gibbs free energy G of different phases, and identify the phase boundary as PT conditions with equal G. The Gibbs free energy is defined as

$$G = F + PV, \tag{1}$$

where F stands for the Helmholtz free energy, V is the volume, and the pressure P is related to F as

$$P = -\left(\frac{\partial F}{\partial V}\right)_T. \tag{2}$$

The Helmholtz free energy is defined to be

$$F = E - TS, \tag{3}$$

where E denotes the internal energy, and S represents the entropy, which for metal systems includes contributions from lattice vibrations and electronic excitations $S_{\rm vib}$ and $S_{\rm el}$. According to Eqs. (1) and (2), once F as a function of V and T is known, G as a function of P and T can be straightforwardly evaluated.

QHA is routinely employed to compute the free energy of solid phases at relatively low temperatures, when anharmonic effects are small. Within QHA, the harmonic vibrational properties as a function of temperature can be evaluated using the phonon-gas model (PGM) [36] as

$$E^{\rm h}_{\rm vib}(T) = \sum_{\mathbf{q}s}\left[\frac{\hbar\omega_{\mathbf{q}s}}{2} + \frac{\hbar\omega_{\mathbf{q}s}}{\exp(\hbar\omega_{\mathbf{q}s}/k_BT) - 1}\right] \tag{4}$$

and

$$S^{\rm h}_{\rm vib}(T) = k_B\sum_{\mathbf{q}s}\left\{\frac{\hbar\omega_{\mathbf{q}s}/k_BT}{\exp(\hbar\omega_{\mathbf{q}s}/k_BT) - 1} - \ln\left[1 - \exp\left(-\frac{\hbar\omega_{\mathbf{q}s}}{k_BT}\right)\right]\right\}, \tag{5}$$

where the superscript "h" stands for "harmonic," the subscript "vib" denotes "vibrational," $\hbar$ is the Planck constant divided by 2π, k_B is the Boltzmann constant, and $\omega_{\mathbf{q}s}$ represents the harmonic phonon frequency for a normal mode $(\mathbf{q}, s)$, $\mathbf{q}$ being a wave vector in the Brillouin zone and s denoting a phonon branch. $\omega_{\mathbf{q}s}$ can be computed using the density-functional perturbation theory (DFPT) [37]. Consistently with Eq. (3), in QHA the Helmholtz free energy can be expressed as

$$F_{\rm QHA}(T) = \left[E_0 + E^{\rm h}_{\rm vib}(T)\right] - T\left[S^{\rm h}_{\rm vib}(T) + S_{\rm el}\right], \tag{6}$$

where E_0 represents the static ground-state energy. The electronic entropy can be calculated using the Mermin functional [38,39] as

$$S_{\rm el} = -k_B\int n(\epsilon)[f\,\ln f + (1-f)\ln(1-f)]d\epsilon, \tag{7}$$

where $n(\epsilon)$ is the electronic density of states, and f is the corresponding electronic occupancy described by the Fermi-Dirac distribution. In order to achieve a rigorous evaluation of $F_{\rm QHA}(T)$, E_0, $\omega_{\mathbf{q}s}$, and $S_{\rm el}$ should all be calculated at the same electronic temperature $T_{\rm el} = T$, as we do in this work. As a result, the harmonic phonon frequencies of metal systems

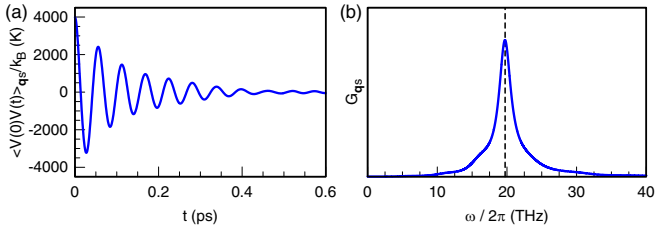

FIG. 1. (a) VACF of an optical phonon mode $(\mathbf{q}, s)$ at $\mathbf{q} = \Gamma$ with a harmonic frequency $\omega/2\pi = 22.8$ THz, for hcp Be at $V = 4.6$ Å^3/atom and $T = 4000$ K. (b) The corresponding power spectrum, obtained by Fourier transforming the VACF to the frequency domain using the maximum entropy method (MEM) [42]. The vertical dashed line indicates the anharmonic frequency $\tilde{\omega}/2\pi = 19.7$ THz.

would exhibit some dependence on $T_{\rm el}$, usually very weak (see, e.g., Supplemental Material of Ref. [32]).

Anharmonicity becomes more prominent as temperature rises, and at high temperatures it may be strong enough to significantly influence thermodynamic properties as well as phase stability. In this work, a recently developed vibrational normal mode analysis method [30,31] is employed to account for anharmonic contributions to lattice vibrations. This is a hybrid approach which extracts knowledge of lattice anharmonicity from first-principles MD with the assistance of LD, through characterization of phonon quasiparticles [40,41]. Such characterization simplifies the original sophisticated problem of fully interacting anharmonic phonons to an effective system of noninteracting phonon quasiparticles, such that to a large extent the PGM can still be applied. The existence of well-defined phonon quasiparticle can be verified by analyzing the mode-projected velocity autocorrelation function (VACF), which for a system of N atoms is defined as

$$\langle V(0)V(t)\rangle_{\mathbf{q}s} = \lim_{\tau\to\infty}\frac{1}{\tau}\int_0^\tau V^*_{\mathbf{q}s}(t')V_{\mathbf{q}s}(t'+t)dt', \quad (8)$$

where $V_{\mathbf{q}s}(t) = \sum_{i=1}^{N}[\sqrt{m_i}\exp(i\mathbf{q}\cdot\mathbf{R}_i)\mathbf{v}_i(t)\cdot\mathbf{e}^i_{\mathbf{q}s}]$ is the mass-weighted and mode-projected velocity for a normal mode $(\mathbf{q}, s)$, $\mathbf{q}$ being commensurate with the supercell size. i denotes the atom index, m_i and $\mathbf{R}_i$ represent the mass and the equilibrium coordinate of the atom, respectively, $\mathbf{v}_i$ is the atomic velocity produced by MD, and $\mathbf{e}^i_{\mathbf{q}s}$ is the polarization vector obtained from LD. The Fourier transform of the VACF gives the corresponding power spectrum as

$$G_{\mathbf{q}s}(\omega) = \int_0^\infty \langle V(0)V(t)\rangle_{\mathbf{q}s}\exp(i\omega t)dt. \quad (9)$$

As an example, Fig. 1 illustrates the VACF and the power spectrum of an optical mode $(\mathbf{q}, s)$ at the Γ point in the Brillouin zone with a harmonic frequency $\omega/2\pi = 22.8$ THz, for hcp Be at the thermodynamic state $V = 4.6$ Å^3/atom and $T = 4000$ K. The VACF displays a nicely decaying oscillatory behavior and the corresponding power spectrum possesses a single Lorentzian-type line shape, indicating that phonon quasiparticle is well defined for this mode [30,31]. For a well-defined phonon quasiparticle, the anharmonic phonon frequency is given by the peak position, in this case as $\tilde{\omega}/2\pi = 19.7$ THz, and the corresponding phonon lifetime is inversely proportional to the linewidth (width at half height of the peak). Here, we can see that as a result of anharmonic effects, the phonon frequency acquires a temperature dependence, and the corresponding lifetime is no longer infinite as that of harmonic phonons.

The small supercell employed in first-principles MD may lead to anharmonic frequencies on a $\mathbf{q}$ grid that is not dense enough for converged calculations of vibrational properties. To make evaluations corresponding to the thermodynamic limit $N\to\infty$, anharmonic frequencies at any $\mathbf{q}$ point in the Brillouin zone can be obtained via Fourier interpolation [30,31], in a way similarly to that routinely done for harmonic phonons. When using anharmonic frequencies $\tilde{\omega}_{\mathbf{q}s}$ to evaluate vibrational properties with anharmonic contributions, the PGM formula for entropy is still valid:

$$S_{\rm vib}(T) = k_B\sum_{\mathbf{q}s}\left\{\frac{\hbar\tilde{\omega}_{\mathbf{q}s}(T)/k_BT}{\exp[\hbar\tilde{\omega}_{\mathbf{q}s}(T)/k_BT]-1} - \ln\left[1-\exp\left(-\frac{\hbar\tilde{\omega}_{\mathbf{q}s}(T)}{k_BT}\right)\right]\right\}, \quad (10)$$

while that for internal energy is not [36,41]. The internal energy with anharmonic vibrational contribution, however, can be readily obtained from direct MD output. Theoretical derivations proved that Eq. (10) is accurate to second order in anharmonic perturbation theory [36,43,44], and perhaps even beyond [45]. Meanwhile, calculations demonstrated that the vibrational entropy computed in this approximated approach agrees excellently with that obtained using the formally exact (but computationally demanding) thermodynamic integration technique, even at very high temperatures, for simple [41] as well as complex systems [30,31]. With anharmonic effects considered in MD, the Helmholtz free energy as a function of temperate can be evaluated via a numerical integration of entropy [30]

$$F(T) = E_0 + \frac{1}{2}\sum_{\mathbf{q}s}\hbar\omega_{\mathbf{q}s} - \int_0^T [S_{\rm el}(T') + S_{\rm vib}(T')]dT', \quad (11)$$

where the second term on the right-hand side is the zero-point correction to the static energy E_0 [given by Eq. (4) with $T = 0$], and $S_{\rm el}(T)$ can be obtained from direct MD output, as the average over values calculated at each instantaneous time step using Eq. (7). Application of this equation is not always convenient since small errors from $S_{\rm el}$ and $S_{\rm vib}$ can accumulate along the integration path, leading to large errors in the calculated F at high T. According to the definition $F = E - TS$, F can be evaluated alternatively as

$$F(T) = E(T) - T[S_{\rm el}(T) + S_{\rm vib}(T)], \quad (12)$$

where like $S_{\rm el}(T)$, the internal energy $E(T)$ can also be obtained from direct MD output. Since ionic motions are always treated classically in MD, quantum effects, which might be important at low T, are automatically neglected in the vibrational contributions to $E(T)$. To fully account for quantum effects, an approximate correction can be applied to $E(T)$ following Lin *et al.* [46]:

$$\Delta E_{\rm qc}(T) = \hat{E}_{\rm vib}(T) - 3(N-1)k_BT, \quad (13)$$

where the effective quantum vibrational energy $\hat{E}_{\rm vib}$ is calculated with Eq. (4) by replacing $\omega_{\mathbf{q}s}$ with $\tilde{\omega}_{\mathbf{q}s}$, and the second term on the right-hand side represents the classical vibrational energy of harmonic oscillators. $\Delta E_{\rm qc}$ has the correct asymptotic behavior in temperature, that at $T = 0$ K it equals the zero-point vibrational energy, and at $T \to \infty$ it approaches zero.

Wherein a thermodynamic property has been determined from both QHA and MD, the anharmonic contributions to it can be evaluated as the total value obtained from MD minus the harmonic counterpart obtained from QHA, e.g., $S^{\rm ah}_{\rm vib}(T) = S_{\rm vib}(T) - S^{\rm h}_{\rm vib}(T)$, where the superscript "ah" means "anharmonic."

III. COMPUTATIONAL DETAILS

First-principles simulations were carried out using the projected-augmented-wave (PAW) method [47,48], as implemented in the Vienna *ab initio* simulation package (VASP) [49–51] and the in-house *ab initio* plane-wave code CESSP [52–54] developed on the infrastructure JASMIN [55]. The exchange-correlation (XC) interaction was described by the generalized gradient approximation of Perdew, Burke, and Ernzerhof (PBE) [56]. The basis set included plane waves up to a kinetic energy cutoff of 350 eV. Calculations with two valence electrons were performed, which yield a static hcp/bcc transition pressure (without zero-point correction) of about 408 GPa, only slightly lower than that calculated with four valence electrons (less than 3% difference). Electronic excitations were taken into account by the Mermin functional formalism [38,39] and electronic smearing at $T = 0$ K was handled by a first-order Methfessel-Paxton method [57] with a smearing width of 0.2 eV.

Harmonic phonon frequencies were computed with DFPT [37], and anharmonic ones were extracted from MD by performing vibrational normal mode analysis [30,31]. $4 \times 4 \times 4$ supercells containing 128 atoms were employed for hcp and bcc Be. To account for size effects, the vibrational properties computed from PGM were evaluated with phonon frequencies interpolated to a $64 \times 64 \times 64$ q mesh, corresponding to calculations performed in a $64 \times 64 \times 64$ supercell. The interpolation has non-negligible effects on the MD results at high temperatures, where it is found to lower the stability of hcp Be relative to bcc Be. For example, at $V = 4.6$ Å^3/atom and $T = 4000$ K, after interpolation the vibrational entropic contribution to the free energy, $-TS_{\rm vib}$, of hcp and bcc Be decreases by 11.9 and 13.4 meV/atom, respectively, leading to a net increase of 1.5 meV/atom in the free energy of hcp Be relative to bcc Be. By comparing with simulations performed in larger supercells, size effects on the vibrational contributions to the internal energy were found to be trivial in MD, and therefore would not be considered. The Brillouin zone of the supercell was sampled with a dense Γ-centered k-mesh setting $5 \times 5 \times 3$ for hcp Be and $4 \times 4 \times 4$ for bcc Be, unless otherwise explicitly stated. We will demonstrate in Sec. IV D that such dense sampling is essential to achieve desirable accuracy in the calculated free energy, for the accurate determination of the high-pressure hcp/bcc phase boundary.

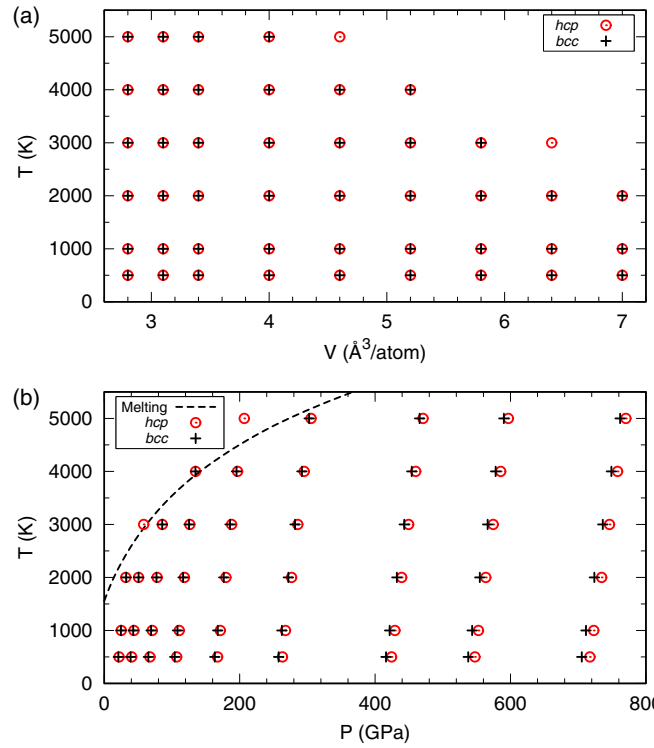

FIG. 2. V-T (a) and P-T (b) conditions covered in our MD simulations for hcp and bcc Be. The melting line in (b) is adopted from Robert *et al.* [20].

Born-Oppenheimer MD simulations were conducted under the NVT (constant particle number, constant volume, and constant temperature) ensemble with ionic temperature controlled by the Nosé thermostat [58]. The time step was chosen to be 1 fs. Each simulation first ran for at least 2 ps to reach thermal equilibrium, and then continued for another 10 ps to collect statistics. As shown in Fig. 2, our MD simulations cover a wide range of thermodynamic conditions: nine volumes from 2.8 to 7.0 Å^3/atom and six temperatures from 500 to 5000 K, with the corresponding pressure extending from about 20 to 770 GPa.

For a given volume, the variation of the c/a ratio of hcp Be with temperature is found to be very small, less than 1% at the highest temperatures considered. For convenience, in our calculations the c/a ratio at $T = 0$ K is considered to be invariant along the isochore. Such a treatment has marginal effect on the calculated free energy of hcp Be, which results in a maximum overestimation below 1 meV/atom.

IV. RESULTS AND DISCUSSIONS

A. Phonon dispersion

In this work, the reliable determination of phase boundary depends on the accurate calculation of vibrational properties, more specifically, the vibrational frequencies. We computed harmonic phonon frequencies at zero temperature with DFPT [37], and extracted anharmonic ones at nonzero temperatures from MD by performing vibrational normal mode analysis [30,31] as described in Sec. II. In Fig. 3, excellent agreement

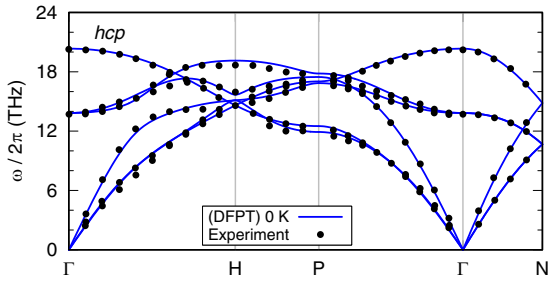

FIG. 3. Calculated harmonic phonon dispersion of hcp Be at the static equilibrium volume $V_0 = 8.08$ Å^3/atom (with zero-point energy considered in determining V_0), in comparison with neutron scattering data measured at $T = 80$ K [59].

is found between the calculated harmonic phonon dispersion of hcp Be with neutron scattering data measured at $T = 80$ K [59]. Typical examples for the evolution of the phonon dispersion of hcp and bcc Be with temperature and volume are presented in Figs. 4 and 5. In accordance with the convergence of free energy and phase boundary (see Sec. IV D), it is more difficult to reach the convergence with respect to k-mesh sampling for the harmonic dispersion at $T = 0$ K than for the anharmonic ones at high T. Therefore, to ensure the convergence, the harmonic phonon dispersions reported in Figs. 3, 4, and 5 were all obtained with a dense $10 \times 10 \times 10$ k mesh for both hcp and bcc Be. For the phonon dispersion at a specific VT condition, the corresponding pressure obtained from MD can be found in Fig. 2.

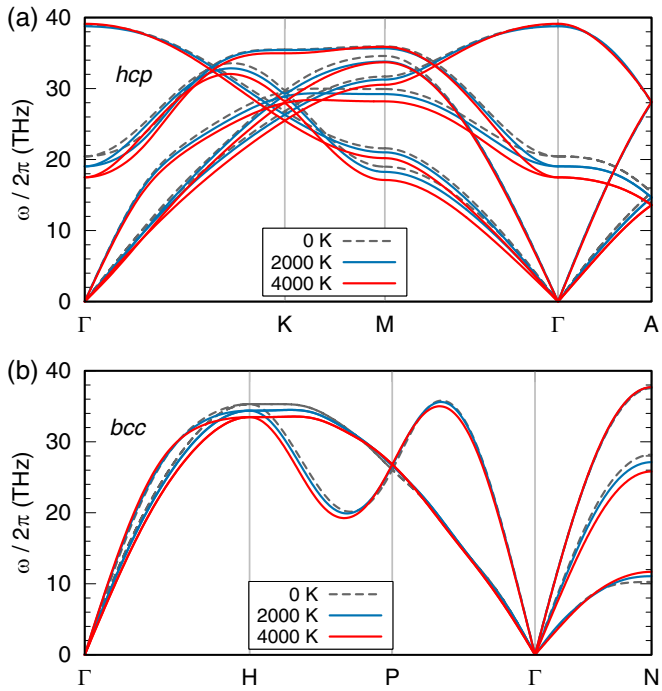

FIG. 4. Evolution of the phonon dispersion of hcp (a) and bcc (b) Be with temperature for $V = 4.6$ Å^3/atom, along high-symmetry directions in the Brillouin zone.

In Fig. 4, the phonon dispersions are compared at three temperatures, $T = 0$, 2000, and 4000 K, for a given volume $V = 4.6$ Å^3/atom. As T rises, the anharmonic dispersion deviates more from the harmonic counterpart, and the differences become noticeable at a few thousand kelvin, showing the importance of anharmonic effects at high T. We observe that the frequency shift with T displays diversified trends, where for a specific normal mode $(\mathbf{q}, s)$ at any $\mathbf{q}$ point in the Brillouin zone it can be positive, negative, or almost zero, indicating the complexity of lattice anharmonicity. This observation is in consistency with previously reported by Lu *et al.* for hcp and bcc Be at low pressures ($P < 30$ GPa) [32].

In Fig. 5, the phonon dispersions are compared at three volumes, $V = 3.4$, 4.6, and 5.8 Å^3/atom, for both the anharmonic dispersion at $T = 3000$ K and the harmonic counterpart at $T = 0$ K. Both the harmonic and anharmonic frequencies decrease with V; and, moreover, the differences between harmonic and anharmonic dispersions grow with V, suggesting that anharmonic effects are stronger at larger volumes. These behaviors are due to the weaker interatomic interactions at larger volumes, which decrease vibrational frequencies and enlarge lattice anharmonicity.

According to previous calculations, imaginary phonon frequencies emerge in the harmonic dispersion of bcc Be at large volumes, e.g., at $V > 7.1$ Å^3/atom (corresponding to $P < 11$ GPa at $T = 0$ K) as predicted by Robert *et al.* [20], indicating dynamic instability of the bcc structure at zero and also low temperatures [60]. Kádas *et al.* suggested that the appearance of imaginary phonon frequencies in bcc Be might be closely related to an electronic topological transition driven by sp hybridization [16]. Based on vibrational normal mode analysis, Lu *et al.* showed that bcc Be is dynamically stabilized by anharmonic effects at low P-high T conditions ($0 < P < 11$ GPa and $1000 < T < 2000$ K) [32]. In contrast to the cases at low pressures, we find that hcp and bcc Be are dynamically stable for all the thermodynamic states investigated by MD in this study (see Fig. 2), as well as for the corresponding zero-temperature states, with no appearance of imaginary phonon frequencies in the calculated harmonic and anharmonic dispersions.

B. Vibrational entropy

The harmonic and total vibrational entropy $S^{\mathrm{h}}_{\mathrm{vib}}$ and S_{vib} can be computed using Eqs. (5) and (10) from harmonic and anharmonic vibrational frequencies, respectively. As discussed in Sec. II, the S_{vib} computed using Eq. (10) can capture the great majority of lattice anharmonicity, even at very high temperatures, and therefore is expected to be sufficiently accurate for the purpose of this work. Of course, the ideal case would be to benchmark our calculated results against the formally exact thermodynamic integration approach. However, such benchmarks are computationally quite involved and beyond this paper, as a result will be considered in our future work on beryllium. In Fig. 6, we report the total vibrational entropy of hcp and bcc Be as a function of temperature at three volumes $V = 3.4$, 4.0, and 4.6 Å^3/atom, as well as the corresponding anharmonic vibrational entropy determined as $S^{\mathrm{ah}}_{\mathrm{vib}} = S_{\mathrm{vib}} - S^{\mathrm{h}}_{\mathrm{vib}}$. The lines which indicate trends of the calculated data

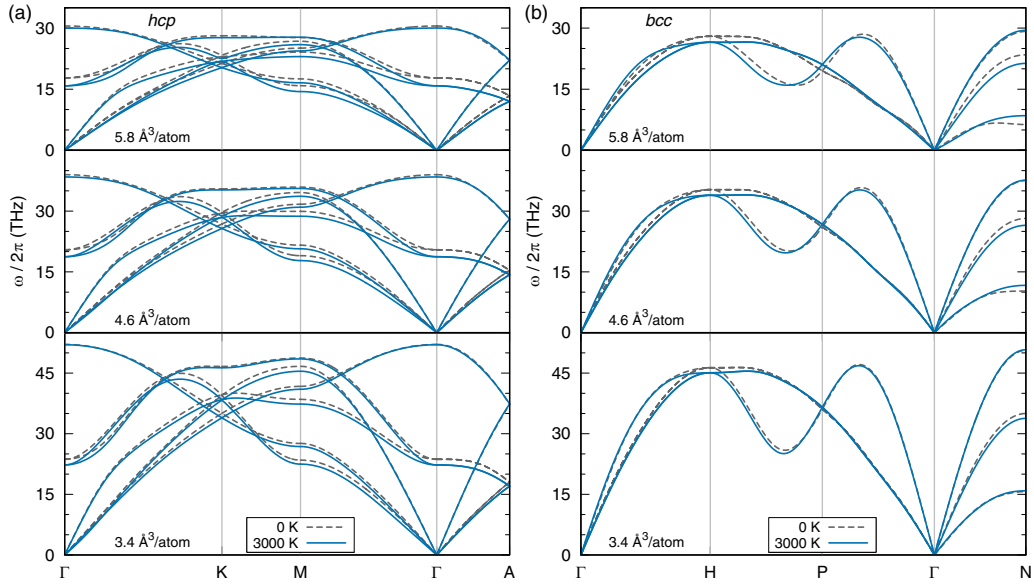

FIG. 5. Evolution of the phonon dispersion of hcp (a) and bcc (b) Be with volume, along high-symmetry directions in the Brillouin zone. Both the harmonic dispersion at $T = 0$ K and the anharmonic one at $T = 3000$ K are shown.

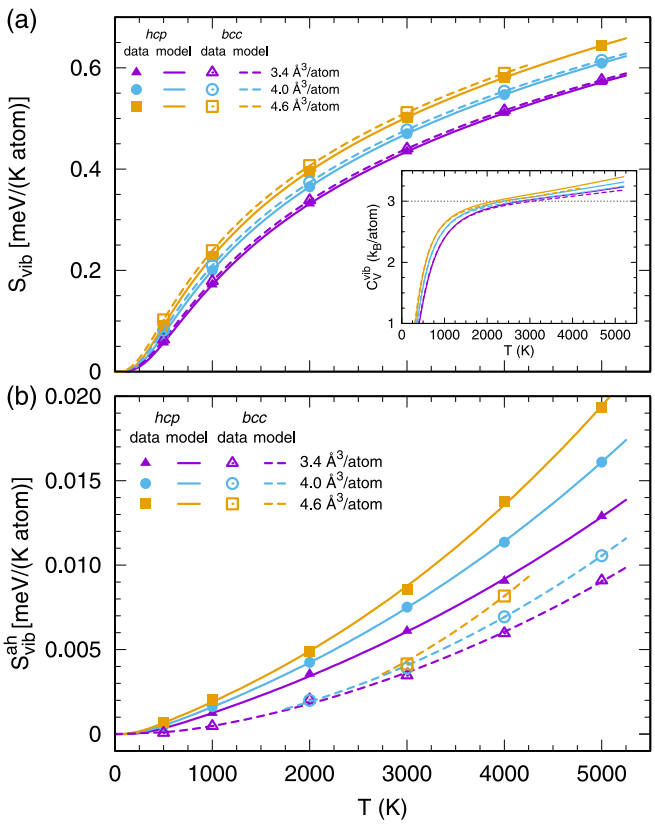

FIG. 6. (a) Total vibrational entropy of hcp and bcc Be as a function of temperature at selected volumes. The inset of (a) illustrates the vibrational heat capacity determined from the total vibrational entropy. (b) The corresponding anharmonic vibrational entropy. Results are not shown for bcc Be in the deep metastable regime. In (a) and (b), symbols represent the calculated data, and lines are results evaluated from model calculations (see text).

are results from model calculations, obtained by fitting the frequency of each normal mode to a second-order polynomial in T, for the subsequent evaluation of temperature-dependent vibrational entropy [30,32]. For $S_{\rm vib}^{\rm ah}$, the slight discrepancies between the lines and the calculated data reflect small computational errors due to finite MD simulation time.

Figure 6(a) shows that the total vibrational entropy $S_{\rm vib}$ increases monotonously with V and T. The same is true for the harmonic counterpart $S_{\rm vib}^{\rm h}$. At nonzero temperatures, the vibrational entropy of bcc Be is larger than that of hcp Be, for both $S_{\rm vib}$ and $S_{\rm vib}^{\rm h}$. According to Eq. (11), this makes the bcc phase energetically more and more favorable compared with the hcp phase as T rises. In the inset of Fig. 6(a), we report the vibrational heat capacity $C_V^{\rm vib}$ determined as $C_V^{\rm vib} = (\partial S_{\rm vib}/\partial T)_V$, based on our model calculations for the temperature dependence of $S_{\rm vib}$. $C_V^{\rm vib}$ is found to go beyond the Dulong-Petit limit 3 k_B/atom at high T, for both hcp and bcc Be. This demonstrates that at high T anharmonic effects are strong in both hcp and bcc Be. At high T, the $C_V^{\rm vib}$ of hcp Be is larger than that of bcc Be, indicating more pronounced lattice anharmonicity in hcp Be. Note that $C_V^{\rm vib}$ can reach 3.3 k_B/atom before solid beryllium melts (see Fig. 2 for the thermodynamic condition at melting).

The anharmonic vibrational entropy $S_{\rm vib}^{\rm ah}$ is a small fraction of the harmonic and total ones. As shown in Fig. 6(b), $S_{\rm vib}^{\rm ah}$ has a general tendency to increase with V and T. This shows quantitatively that anharmonic effects are stronger at larger volumes and higher temperatures, in accordance with previous discussions associated with Figs. 4 and 5 for the phonon dispersions. At high T, the $S_{\rm vib}^{\rm ah}$'s of hcp and bcc Be, and also the difference between them, can even become comparable to the entropy change upon hcp/bcc transition at low pressures ($P < 11$ GPa), $S_{\rm bcc} - S_{\rm hcp} = 0.0181$ meV/(K atom) [32]. This suggests that anharmonicity can have a significant effect on the hcp/bcc transition at high-PT conditions.

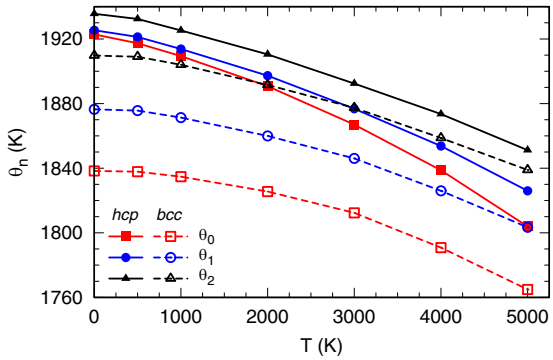

FIG. 7. θ_0, θ_1, and θ_2 of hcp and bcc Be as a function of temperature for $V = 4.0$ Å^3/atom. θ_0, θ_1, and θ_2 are frequency moments of the PDOS (see text). Symbols represent the calculated data, and lines are guides for the eye.

We will see in Sec. IV E that it is indeed the case. The anharmonic vibrational entropy of hcp Be is larger than that of bcc Be, which clearly shows that anharmonic effects are more pronounced in hcp Be than in bcc Be. As a consequence, lattice anharmonicity reduces the free energy of hcp Be more than that of bcc Be according to Eq. (11), and therefore would enlarge the stability domain of hcp Be while diminishing that of bcc Be. Stronger anharmonic effects in hcp Be are also visible in the mean-square displacement (MSD). Compared with that of bcc Be, as T rises the MSD of hcp Be is found to exhibit a larger deviation from the harmonic case, where the MSD increases perfectly linearly with increasing T [61].

To understand microscopically why the anharmonic vibrational entropy is larger in hcp Be than in bcc Be, we compute three phonon characteristic temperatures that correspond to different frequency moments of the phonon density of states (PDOS) [44]

$$\ln(k_B\theta_0) = \langle \ln(\hbar\tilde{\omega})\rangle_{\mathrm{BZ}}; \quad k_B\theta_1 = \tfrac{4}{3}\langle \hbar\tilde{\omega}\rangle_{\mathrm{BZ}};$$
$$k_B\theta_2 = \left[\tfrac{5}{3}\langle(\hbar\tilde{\omega})^2\rangle_{\mathrm{BZ}}\right]^{1/2}, \tag{14}$$

where $\tilde{\omega}$ represents the temperature-dependent vibrational frequency, and $\langle\ldots\rangle_{\mathrm{BZ}}$ denotes average over the Brillouin zone. θ_0, θ_1, and θ_2 are measures of the vibrational frequencies averaged in different ways, and are closely related to the vibrational properties, including the vibrational entropy. In Fig. 7, θ_0, θ_1, and θ_2 are compared between hcp and bcc Be, as a function of temperature for a given volume $V = 4.0$ Å^3/atom. The θ_0, θ_1, and θ_2 of hcp and bcc Be all decrease with increasing T. This means that although the frequency shift with T can display diversified trends for a single mode, the average effect of lattice anharmonicity is the decrease of vibrational frequencies with increasing T. According to Eq. (10), for a given temperature smaller vibrational frequencies would lead to a larger total vibrational entropy, and thus equivalently to a larger anharmonic vibrational entropy. For all of θ_0, θ_1, and θ_2, as T rises the value of hcp Be drops faster than that of bcc Be, which explains the larger anharmonic vibrational entropy of hcp Be. The stronger anharmonic effects on the frequency shifts observed in hcp Be may be attributed to the intrinsic anisotropy of the hcp structure. Moreover, it can be noted that θ_0, θ_1, and θ_2 all drop increasingly faster at higher temperatures, which makes it clear why in Fig. 6(b) the anharmonic vibrational entropy grows increasingly faster at higher temperatures.

C. Free energy with anharmonic contributions

Through direct simulation of atomic motions at finite temperatures, anharmonic contributions to thermodynamic properties are automatically taken into account in MD. According to Eqs. (1) and (12), in addition to the vibrational entropy S_{vib} considered in the previous subsection, the calculation of the Gibbs free energy G from MD, and the subsequent determination of phase boundary as well, requires to know the internal energy E, the pressure P, and the electronic entropy S_{el}. Fortunately, E, P, and S_{el} can all be straightforwardly obtained from direct MD output. S_{el} is generally quite small; at the highest temperatures considered, it is determined to be less than 2% of S_{vib}, for both hcp and bcc Be. The anharmonic contributions to S_{el} are much smaller compared with those to S_{vib}, nevertheless, they are explicitly accounted for in our MD simulations.

In Fig. 8, we report the internal energy and pressure of hcp and bcc Be obtained from our MD simulations, as a function of volume at selected temperatures. As shown in the figure, for a given temperature the volume dependence of E and P can be well fitted to the fourth-order Birch-Murnaghan equation of state (EOS) [62]. Each fitting parameter can be properly described by a third-order polynomial in T to obtain unified functional descriptions of E and P, i.e., $E(V,T)$ and $P(V,T)$, which can be used to evaluate derived thermodynamic properties. From the inset of Fig. 8(a), we see that at small volumes, e.g., $V \leqslant 4.6$ Å^3/atom (the corresponding $P > 160$ GPa), the absolute energy difference between two phases is considerably smaller than that at large volumes, e.g., $V \geqslant 7.0$ Å^3/atom (the corresponding $P < 40$ GPa). This suggests the difficulty for the theoretical identification of energetically more stable structure at high pressures.

According to Eq. (12), the Helmholtz free energy F is calculated from MD using E, S_{vib}, and S_{el}. In Fig. 9(a), F as a function of volume is presented at selected temperatures for hcp and bcc Be. Similarly to E and P, for a given temperature the volume dependence of F can be well described by the fourth-order Birch-Murnaghan EOS for energy [62]. According to definition, the Gibbs free energy is computed as $G = F + PV$. In Fig. 9(b), the Gibbs free-energy difference $\Delta G = G_{\mathrm{bcc}} - G_{\mathrm{hcp}}$ is shown as a function of pressure at selected temperatures. For a given temperature ΔG decreases monotonously with pressure, and the point at which $\Delta G = 0$ gives the transition pressure $P_{\mathrm{hcp/bcc}}$ at the considered temperature. $P_{\mathrm{hcp/bcc}}$ decreases with increasing T, which leads to smaller stability domain of the hcp phase or, equivalently, larger stability domain of the bcc phase, at higher temperatures. This is attributed to the fact that the entropy associated with the more symmetric bcc structure is larger than that of the hcp structure (see Fig. 6). The full hcp/bcc phase line at high pressures will be presented in Sec. IV E.

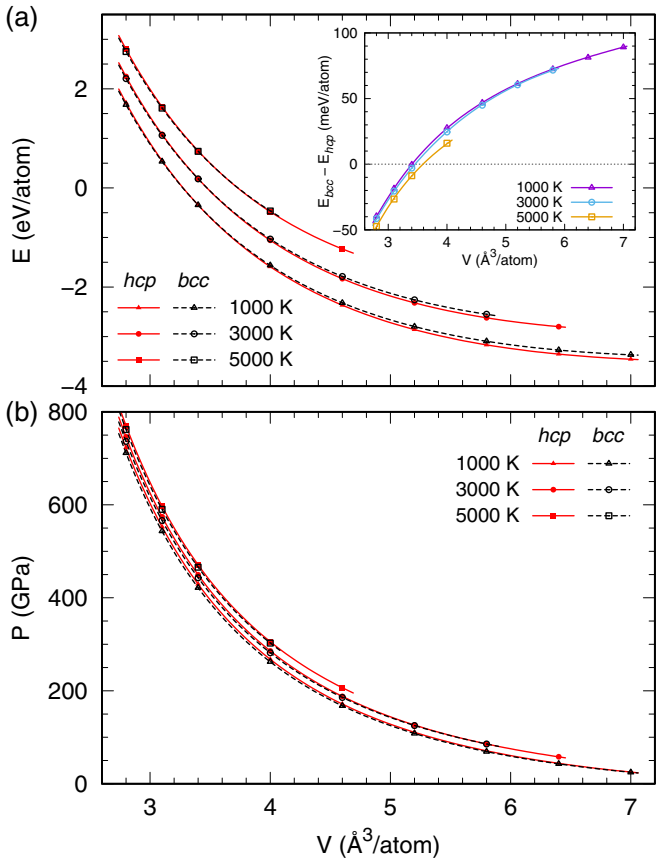

FIG. 8. Internal energy (a) and pressure (b) of hcp and bcc Be obtained from MD, as a function of volume at selected temperatures. Symbols represent the calculated data, and lines are fits to the fourth-order Birch-Murnaghan EOS [62]. Inset in (a): the corresponding internal energy difference between hcp and bcc Be.

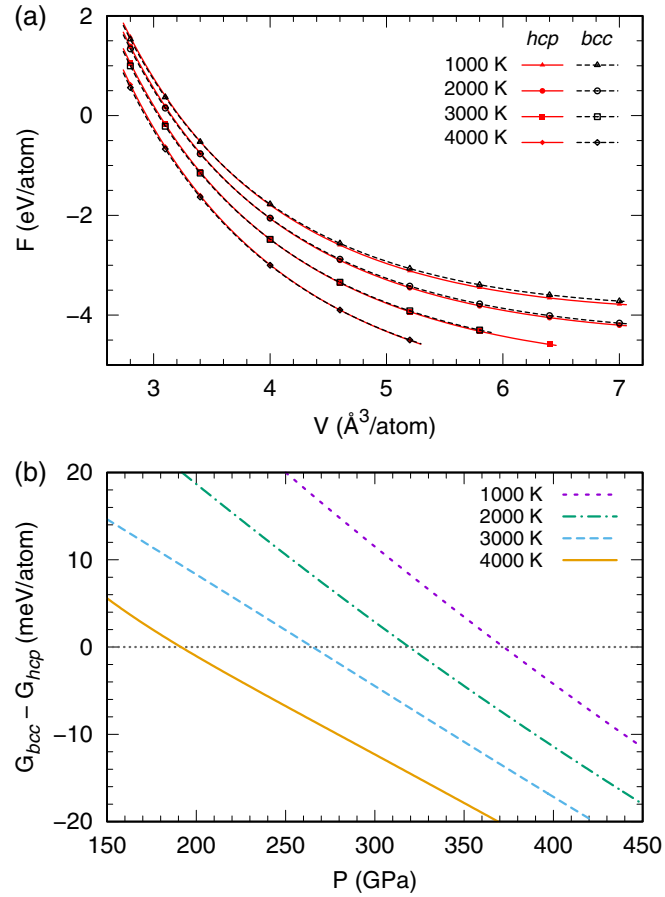

FIG. 9. (a) Helmholtz free energy of hcp and bcc Be obtained from MD, as a function of volume at selected temperatures. Symbols represent the calculated data, and lines are fits to the fourth-order Birch-Murnaghan EOS [62]. (b) The corresponding Gibbs free-energy difference between hcp and bcc Be.

D. Importance of free energy and phase boundary convergence with respect to *k*-mesh sampling

Before presenting the final results for the phase diagram of beryllium, we would like to discuss an important technical detail that should be paid particular attention to, the k-mesh setting. Through thorough tests, we find that the calculated free energy depends sensitively on the k mesh, and therefore it is necessary to employ a dense setting to achieve desirable accuracy in the calculated phase boundary. In our calculations with 128-atom supercells, the least requirement is $5 \times 5 \times 3$ for hcp Be and $4 \times 4 \times 4$ for bcc Be, which are the setting employed to obtain all the MD results presented up to now.

In Fig. 10, we report the harmonic and total Helmholtz free energy of hcp and bcc Be, computed with different k meshes at a low temperature $T = 500$ K and a high temperature $T = 4000$ K, for a given volume $V = 4.6$ Å^3/atom. The harmonic and total Helmholtz free energy are obtained from QHA and MD, respectively. The k meshes considered are all Γ centered, varying from as sparse as Γ point only in both QHA and MD, up to as dense as $10 \times 10 \times 10$ in QHA, and $5 \times 5 \times 3$ for hcp and $4 \times 4 \times 4$ for bcc in MD. At both temperatures, the k-mesh dependence of the Helmholtz free energy calculated from MD displays a quite analogous trend as that from QHA, for both hcp and bcc Be, indicating that the convergence behavior is basically not influenced by anharmonicity. As shown in the figure, the Helmholtz free energy is easier to converge at higher temperatures: Using the same $3 \times 3 \times 3$ k mesh and taking the well-converged $10 \times 10 \times 10$ k-mesh results as references, the QHA value at $T = 4000$ K converges to within 2 and 1 meV/atom, while that at $T = 500$ K is about 7 and 4 meV/atom from convergence, for hcp and bcc Be, respectively. The better convergence at $T = 4000$ K is because of the larger width of electronic smearing corresponding to higher temperatures. For the same reason, faster convergence at higher temperatures is also expected for other thermodynamic properties. We find that a $5 \times 5 \times 3$ k mesh for hcp Be and a $4 \times 4 \times 4$ k mesh for bcc Be can yield good overall convergence of the calculated Helmholtz free energy from QHA, for the volume considered here an overestimation within 2 meV/atom at $T = 500$ K and an underestimation within 0.5 meV at $T = 4000$ K, for both hcp and bcc Be. This k-mesh setting should also lead to satisfactory convergence of the calculated Helmholtz free energy from MD, due to the similar convergence behavior between QHA and MD.

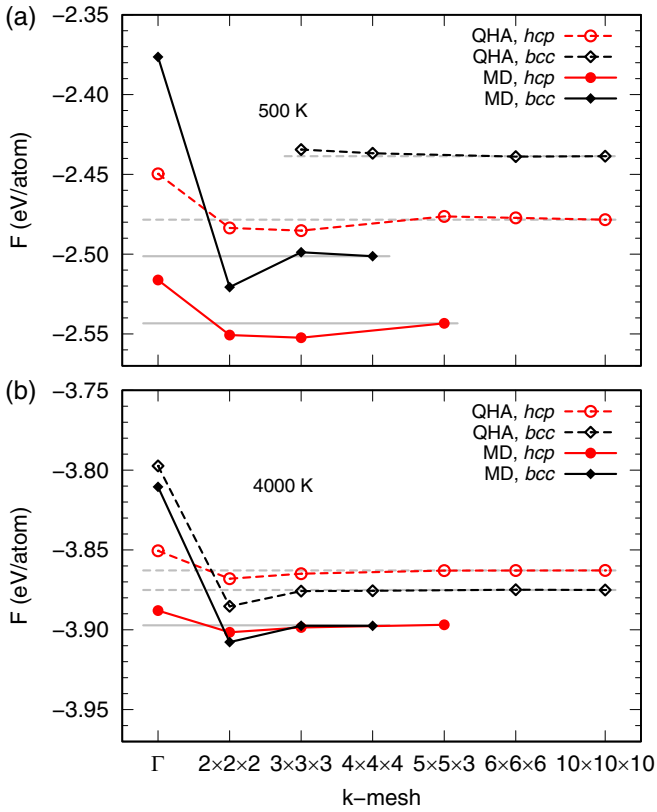

FIG. 10. Convergence of Helmholtz free energy of hcp and bcc Be from QHA and MD with respect to k-mesh sampling, at $T = 500$ K (a) and $T = 4000$ K (b) for $V = 4.6$ Å^3/atom. Lines are guides for the eye. In (a), the QHA values for bcc Be from the Γ only and $2 \times 2 \times 2$ k mesh are not shown since they are not well defined due to emergence of imaginary frequencies in the corresponding harmonic phonon dispersion at $T_{\rm el} = 500$ K.

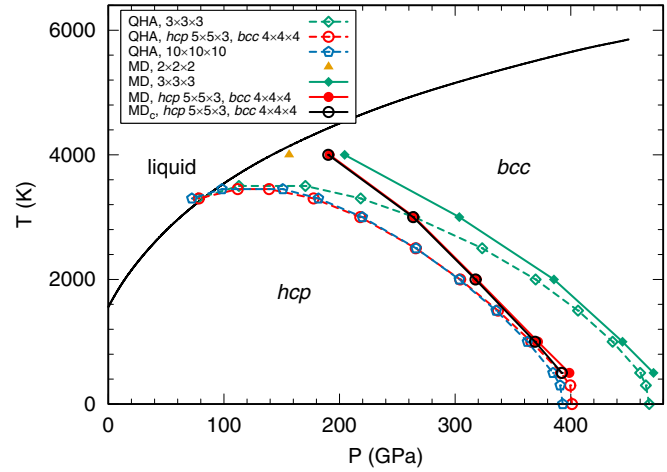

FIG. 11. hcp/bcc phase boundary of beryllium, computed from QHA and MD with different k-mesh settings. "MD$_c$" represents "MD with quantum corrections." When not explicitly specified in the legend, the same k mesh is used for both hcp and bcc Be. Symbols represent the calculated data, and lines between them are guides for the eye. The melting line is adopted from Robert *et al.* [20].

We check directly the convergence of the calculated hcp/bcc phase boundary in Fig. 11, for results from both QHA and MD. The previous subsection has already demonstrated how the phase boundary is determined by comparing the free energy of different phases. The convergence behavior of the phase boundary is consistent with the case shown in Fig. 10 for the Helmholtz free energy: it is similar between QHA and MD, and as T rises the convergence becomes faster due to more converged free energy resulting from larger width of electronic smearing. The discrepancy between the transition pressure determined from a $3 \times 3 \times 3$ k mesh and that from a slightly denser k-mesh setting, $5 \times 5 \times 3$ for hcp and $4 \times 4 \times 4$ for bcc, can be less than 15 GPa at the highest temperatures considered, but increases to be larger than 60 GPa at very low temperatures, for both QHA and MD. This indicates that even a $3 \times 3 \times 3$ k mesh is not sufficient to achieve good overall convergence of the calculated phase boundary, where results are satisfactory only at very high temperatures. (Note that at a very high temperature $T = 4000$ K, even a sparse $2 \times 2 \times 2$ k mesh works much better than a $3 \times 3 \times 3$ k mesh at $T \leqslant 2000$ K.) We find that a slightly denser k-mesh setting, $5 \times 5 \times 3$ for hcp and $4 \times 4 \times 4$ for bcc, already works well in QHA at both low and high temperatures, the discrepancy from a very dense $10 \times 10 \times 10$ k mesh being within 10 GPa at $T = 0$ K and even smaller at higher temperatures. Since a similar behavior is expected in MD, the same k-mesh setting was chosen in our MD simulations to determine the phase boundary with anharmonic contributions. This is clearly much denser than the Γ only or $2 \times 2 \times 2$ k mesh commonly employed in first-principles MD to compute the EOS and thermodynamic properties, but is nearly the most efficient choice to ensure good overall convergence of the calculated phase boundary.

Choosing appropriate k meshes is not only important in this work for beryllium, but may also be crucial for the accurate calculation of the free energy and phase boundary of other materials. Performing convergence tests in MD can be expensive indeed. However, as we have already seen, the convergence behavior with respect to k-mesh sampling is very similar between QHA and MD. Therefore, to save efforts, convergence tests in QHA can serve as useful guides for the selection of appropriate k meshes in MD.

It is worth noting that at $T < 1000$ K, as T declines the MD transition pressure does not seem to approach the QHA one, when compared at the same k-mesh setting. This contradicts the common expectation that anharmonicity becomes weaker at lower temperatures. The problem here is that in MD simulations ionic motions are treated classically following Newton's second law, and quantum corrections to the internal energy are always disregarded. Quantum effects are particularly important for beryllium due to its highest Debye temperature among all metals [2], and should be properly taken into account at relatively low temperatures. An approximate quantum correction to the internal energy given by Eq. (13) can be added to the MD free energy, and the results obtained with the k-mesh setting $5 \times 5 \times 3$ for hcp and $4 \times 4 \times 4$ for bcc are presented in Fig. 11, labeled with "MD$_c$," where a subscript "c" denotes "corrected." As shown in the figure, quantum corrections have

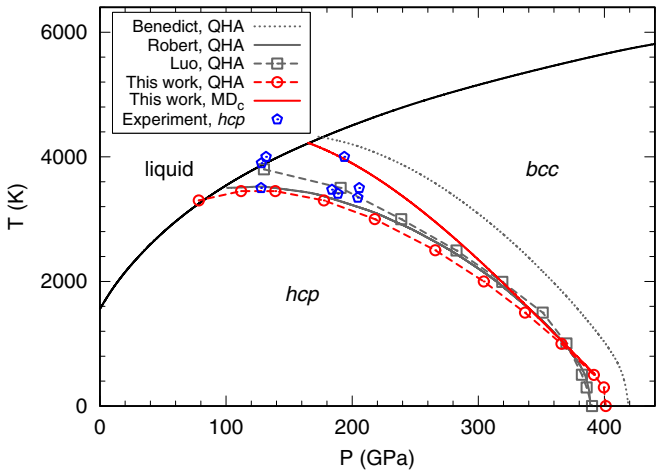

FIG. 12. Phase diagram of beryllium. The hcp/bcc phase boundaries from our QHA and MD_c calculations are compared with those from previous QHA calculations [19–21], where "MD_c" represents "MD with quantum corrections." The uncertainty of the calculated MD_c transition pressure is estimated to be ± 6 GPa at most (see text). The pentagons denote selected high-PT conditions where stable hcp Be was observed to exist in the recent static DAC experiment of Lazicki *et al.* [9]. The experimental uncertainty is about 5 GPa and 100 K for pressure and temperature, respectively, and can be approximately represented by the size of the pentagons. The melting line is adopted from Robert *et al.* [20].

a greater influence at lower temperatures. After considering them, the difference between the MD_c phase boundary and the corresponding QHA one decreases monotonously with decreasing temperature, just as expected. At $T = 500$ K, the MD_c transition pressure is almost identical as the QHA one, indicating that anharmonic effects are almost negligible at $T \leqslant 500$ K.

E. Phase diagram

Figure 12 displays the phase diagram of beryllium, where the hcp/bcc phase boundaries obtained from our QHA and MD calculations are compared with those from previous QHA studies [19–21], and also with recent experimental observations [9]. Compared with the hcp/bcc phase boundary, the melting curve of beryllium seems to be less controversial since despite lack of high-pressure experimental data, first-principles MD studies using different methods all yield consistent results [19,20,63]. The melting curve computed by Robert *et al.* [20] is adopted to constrain the stability domain of solid beryllium. To highlight anharmonic effects, we conduct a direct comparison between our QHA and MD results at the same k-mesh setting, i.e., $5 \times 5 \times 3$ for hcp and $4 \times 4 \times 4$ for bcc, where our MD ones have been applied with quantum corrections as discussed in the previous subsection, labeled as "MD_c" in the figure. By comparing with longer MD simulations of 250 ps, we find that our 10-ps simulations are sufficient to ensure desirable accuracy in the calculated Helmholtz free energy F, to within 0.4 meV/atom at the highest temperatures considered. Taking into account also the small errors resulting from fitting F, we estimate a maximum uncertainty of ± 6 GPa in the calculated hcp/bcc transition pressure from MD. The computational error in QHA is much smaller than that in MD. The hcp/bcc phase boundary at $P < 11$ GPa obtained recently by Lu *et al.* [32], where anharmonic effects were taken into account using the same method [30,31] as for our MD results, lies very close to the melting line, and therefore is not displayed in the figure.

As shown in Fig. 12, overall our QHA phase boundary agrees well with the two latest QHA ones of Robert *et al.* [20] and Luo *et al.* [21], but differs largely from the earlier QHA one of Benedict *et al.* [19]. At $T > 1000$ K, our QHA results agree closely with those of Robert *et al.* computed with the same PBE XC, but display small systematic discrepancies that grow with T from those of Luo *et al.*, which can be attributed to the local-density approximation (LDA) [64] XC used by Luo *et al.* Some small discrepancies can also be found at $T < 1000$ K between our QHA results and those of Robert *et al.* and Luo *et al.* These originate from the fact that our results here were obtained with a sparser k-mesh setting, and the calculated transition pressure converges more slowly with respect to k-mesh sampling at lower temperatures than at higher temperatures (see the previous subsection). When computed with a dense $10 \times 10 \times 10$ k mesh for both hcp and bcc Be, our QHA result at $T = 0$ K is highly consistent with that of Robert *et al.* and Luo *et al.*, all at about 390 GPa (see also Fig. 11). In the PT phase diagram, the stability domain of the hcp phase obtained by Benedict *et al.* using PBE XC is significantly larger than that predicted by the other three QHA calculations. The large discrepancies are attributed to the different transition pressure at $T = 0$ K obtained by Benedict *et al.*, about 420 GPa, which is noticeably larger than that predicted by more recent first-principles calculations, including the other three QHA calculations, in the range of about 380 to 390 GPa [20–23]. After considering lattice vibrations and electronic excitations on top of the $T = 0$ K results by Benedict *et al.*, the discrepancy at $T = 0$ K propagates to higher temperatures. Despite the different transition pressures predicted by Benedict *et al.*, the variation tendency of the transition pressure with temperature, or equivalently the Clapeyron slope, is very similar to the other three QHA calculations. In Fig. 12, we also plot selected high-PT conditions up to which stable hcp Be was observed to exist in the recent static DAC experiment of Lazicki *et al.* [9]. The experimental uncertainty was estimated to be about 5 GPa and 100 K for pressure and temperature, respectively. At $T > 3300$ K, the stability domains of hcp Be predicted by Robert *et al.*, Luo *et al.*, and our QHA calculations are clearly smaller than that observed in experiment, which seems to indicate the importance of anharmonic effects on the high-temperature phase stability.

Figure 12 shows that with anharmonic effects considered, our MD_c phase boundary gives a larger stability domain of hcp Be compared with our QHA one, especially much larger at high T. In particular, the hcp/bcc transition pressure is enlarged by more than 100 GPa at $T \sim 3500$ K, the highest temperature on our QHA phase boundary. The decrease of transition pressure with increasing T in our MD_c results is slower than that in all four QHA calculations, which leads to a Clapeyron slope obviously larger in magnitude at high T predicted by MD_c. Our MD_c phase boundary is consistent with Lazicki *et al.*'s experiment [9]. It incorporates most

experimental points of hcp Be within the calculated stability domain, with only one point lying outside by a distance smaller than both the experimental and the theoretical uncertainties. Note that if our MD simulations were performed with two more valence electrons, and considered the variation of the c/a ratio of hcp Be along the isochore as well, then the calculated stability domain of hcp Be should be further enlarged by at least a few GPa, but not too much more, at high T (see Sec. III). We emphasize that although the position of the calculated hcp/bcc boundary in the phase diagram might differ more or less for different computational details, the conclusion that at high T anharmonicity would significantly enlarge the stability domain of hcp Be is perfectly robust. It is worth noting that the same conclusion may also hold for magnesium, where similarly to beryllium, in recent static experiments [65] the hcp/bcc transition pressure of magnesium at high T was observed to be significantly higher than previously predicted by QHA [66,67].

As a summary, our calculations show that anharmonicity is important at high T. It enlarges the hcp/bcc transition pressure of beryllium by less than 8 GPa (less than 2.5%) at $T < 1500$ K, but by more than 45 GPa (more than 20%) at $T > 3000$ K. Consequently, there is a significant increase in the calculated pressure of the hcp/bcc/liquid triple point, from about 85 to 165 GPa, with the corresponding temperature increasing from about 3300 to 4200 K; and the resulting Clapeyron slope at the triple point takes a value of -7.4 ± 0.7 K/GPa, noticeably larger in magnitude than previous QHA predictions, which are all close to zero and lie in the range of -3 to 2 K/GPa.

V. CONCLUSIONS

We investigated the hcp to bcc phase transition in beryllium at high-PT conditions, where a hybrid approach was employed to account for anharmonic contributions to the free energy. At high T, lattice anharmonicity was shown to be pronounced in both hcp and bcc Be, under the influence of which the vibrational heat capacities can go beyond the Dulong-Petit limit 3 k_B/atom. Anharmonic effects are stronger in hcp Be than in bcc Be, as evidenced by the larger anharmonic vibrational entropy of hcp Be. We found that anharmonicity substantially enlarges the stability domain of hcp Be at high T, bringing calculated results into good consistency with recent experimental observations. Due to anharmonic effects, the calculated pressure and temperature of the hcp/bcc/liquid triple point increase from about 85 to 165 GPa, and from about 3300 to 4200 K, respectively, and the resulting Clapeyron slope at the triple point of -7.4 ± 0.7 K/GPa is noticeably larger in magnitude than previous QHA values in the range of -3 to 2 K/GPa.

An important technical detail was discussed. By performing careful tests we showed that it is necessary to employ a dense k-mesh setting to achieve good overall convergence of the calculated free energy and phase boundary. In our calculations with 128-atom supercells, at least $5 \times 5 \times 3$ for hcp Be and $4 \times 4 \times 4$ for bcc Be are required. This is clearly much denser than the Γ only or $2 \times 2 \times 2$ k mesh commonly employed in first-principles MD to compute the EOS and thermodynamic properties, but is nearly the most efficient choice.

For future perspective, the thermodynamic data of hcp and bcc Be obtained from our QHA and MD calculations are valuable in constructing a multiphase EOS at wide thermodynamic conditions, in both low- and high-temperature regimes [19,20,68–70]. Furthermore, the computational scheme employed in this work can be used to study the high-temperature solid-solid phase transition in other materials, on which anharmonicity may also have significant influences. And, if combined with accurate computational approach for the liquid free energy [46,71,72], this scheme can help to determine the melting curve of solids as well.

ACKNOWLEDGMENTS

This work was supported by Science Challenge Project under Grants No. TZ2016001 and No. TZ2018002, the National Key Research and Development Program of China under Grant No. 2017YFA0403200, the Natural Science Foundation of China under Grants No. 11176002, No. 11474034, No. 11734013, and No. 41474069, and Foundation of LCP under Grant No. 6142A05030204.

[1] K. J. H. Mackay and N. A. Hill, J. Nucl. Mater. **8**, 263 (1963).
[2] A. Migliori, H. Ledbetter, D. J. Thoma, and T. W. Darling, J. Appl. Phys. **95**, 2436 (2004).
[3] D. Swift, D. Paisley, and M. Knudson, in *Proceedings of the Conference of the American Physical Society Topical Group on Shock Compression of Condensed Matter 2013*, edited by M. D. Furnish, Y. M. Gupta, and Jerry W. Forbes, AIP Conf. Proc. No. 706 (AIP, New York, 2004), p. 119
[4] D. S. Clark, S. W. Haan, and J. D. Salmonson, Phys. Plasmas **15**, 056305 (2008).
[5] S. W. Haan *et al.*, Phys. Plasmas **18**, 051001 (2011).
[6] *The Elements*, edited by J. Elmsley (Oxford University Press, London, 1998).
[7] M. Francois and M. Contre, *Conference Internationale sur la Metallurgie du Beryllium* (Universite de France, Grenoble, Paris, 1965).
[8] A. Abey, Lawrence Livermore National Laboratory Report No. UCRL-53567, 1984 (unpublished).
[9] A. Lazicki, A. Dewaele, P. Loubeyre, and M. Mezouar, Phys. Rev. B **86**, 174118 (2012).
[10] R. L. Reichlin, Rev. Sci. Instrum. **54**, 1674 (1983).
[11] H. Olijnyk and A. P. Jephcoat, J. Phys.: Condens. Matter **12**, 8913 (2000).
[12] N. Velisavljevic, G. N. Chestnut, Y. K. Vohra, S. T. Weir, V. Malba, and J. Akella, Phys. Rev. B **65**, 172107 (2002).
[13] K. Nakano, Y. Akahama, and H. Kawamura, J. Phys.: Condens. Matter **14**, 10569 (2002).
[14] W. J. Evans, M. J. Lipp, H. Cynn, C. S. Yoo, M. Somayazulu, D. Häusermann, G. Shen, and V. Prakapenka, Phys. Rev. B **72**, 094113 (2005).
[15] B. Palanivel, R. S. Rao, B. K. Godwal, and S. K. Sikka, J. Phys.: Condens. Matter **12**, 8831 (2000).

[16] K. Kádas, L. Vitos, B. Johansson, and J. Kollár, Phys. Rev. B **75**, 035132 (2007).
[17] G. V. Sin'ko and N. A. Smirnov, Phys. Rev. B **71**, 214108 (2005).
[18] J. Meyer-ter-Vehn and W. Zittel, Phys. Rev. B **37**, 8674 (1988).
[19] L. X. Benedict, T. Ogitsu, A. Trave, C. J. Wu, P. A. Sterne, and E. Schwegler, Phys. Rev. B **79**, 064106 (2009).
[20] G. Robert, P. Legrand, and S. Bernard, Phys. Rev. B **82**, 104118 (2010).
[21] F. Luo, L.-C. Cai, X.-R. Chen, F.-Q. Jing, and D. Alfè, J. Appl. Phys. **111**, 053503 (2012).
[22] Z.-C. Guo, F. Luo, and Y. Cheng, Comput. Mater. Sci. **84**, 139 (2014).
[23] H. Lu, R. Qiu, L. Huang, and T. Tang, Phys. Lett. A **379**, 2479 (2015).
[24] P. Souvatzis, O. Eriksson, M. I. Katsnelson, and S. P. Rudin, Phys. Rev. Lett. **100**, 095901 (2008).
[25] P. Souvatzis, O. Eriksson, M. Katsnelson, and S. P. Rudin, Comput. Mater. Sci. **44**, 888 (2009).
[26] I. Errea, B. Rousseau, and A. Bergara, Phys. Rev. Lett. **106**, 165501 (2011).
[27] I. Errea, M. Calandra, and F. Mauri, Phys. Rev. B **89**, 064302 (2014).
[28] O. Hellman, I. A. Abrikosov, and S. I. Simak, Phys. Rev. B **84**, 180301 (2011).
[29] O. Hellman, P. Steneteg, I. A. Abrikosov, and S. I. Simak, Phys. Rev. B **87**, 104111 (2013).
[30] D.-B. Zhang, T. Sun, and R. M. Wentzcovitch, Phys. Rev. Lett. **112**, 058501 (2014).
[31] T. Sun, D.-B. Zhang, and R. M. Wentzcovitch, Phys. Rev. B **89**, 094109 (2014).
[32] Y. Lu, T. Sun, P. Zhang, P. Zhang, D.-B. Zhang, and R. M. Wentzcovitch, Phys. Rev. Lett. **118**, 145702 (2017).
[33] Y. Lu, F. Zheng, P. Zhang, X. Shao, and D.-B. Zhang, J. Phys.: Condens. Matter **29**, 175701 (2017).
[34] D.-B. Zhang, P. B. Allen, T. Sun, and R. M. Wentzcovitch, Phys. Rev. B **96**, 100302 (2017).
[35] Y. Lu, T. Sun, and D.-B. Zhang, Phys. Rev. B **97**, 174304 (2018).
[36] D. C. Wallace, *Thermodynamics of Crystals* (Dover, New York, 1998).
[37] S. Baroni, S. de Gironcoli, A. Dal Corso, and P. Giannozzi, Rev. Mod. Phys. **73**, 515 (2001).
[38] N. D. Mermin, Phys. Rev. **137**, A1441 (1965).
[39] R. M. Wentzcovitch, J. L. Martins, and P. B. Allen, Phys. Rev. B **45**, 11372 (1992).
[40] A. J. C. Ladd, B. Moran, and W. G. Hoover, Phys. Rev. B **34**, 5058 (1986).
[41] T. Sun, X. Shen, and P. B. Allen, Phys. Rev. B **82**, 224304 (2010).
[42] W. Press, S. Teukolsky, W. Vetterling, and B. Flannery, *Numerical Recipes in Fortran 77: The Art of Scientific Computing* (Cambridge University, Cambridge, 1986).
[43] T. H. K. Barron, in *Lattice Dynamics*, edited by R. F. Wallis (Pergamon, Oxford, 1965), p. 247.
[44] G. Grimvall, *Thermophysical Properties of Materials* (Elsevier, Amsterdam, 1999).
[45] J. C. K. Hui and P. B. Allen, J. Phys. C: Solid State Phys. **8**, 2923 (1975).
[46] S.-T. Lin, M. Blanco, and W. A. Goddard, J. Chem. Phys. **119**, 11792 (2003).
[47] P. E. Blöchl, Phys. Rev. B **50**, 17953 (1994).
[48] G. Kresse and D. Joubert, Phys. Rev. B **59**, 1758 (1999).
[49] G. Kresse and J. Hafner, Phys. Rev. B **47**, 558 (1993).
[50] G. Kresse and J. Hafner, Phys. Rev. B **48**, 13115 (1993).
[51] G. Kresse and J. Furthmüller, Phys. Rev. B **54**, 11169 (1996).
[52] X. Gao, Z. Mo, J. Fang, H. Song, and H. Wang, Comput. Phys. Commun. **211**, 54 (2017).
[53] J. Fang, X. Gao, H. Song, and H. Wang, J. Chem. Phys. **144**, 244103 (2016).
[54] Y. Zhou, H. Wang, Y. Liu, X. Gao, and H. Song, Phys. Rev. E **97**, 033305 (2018).
[55] Z. Mo, A. Zhang, X. Cao, Q. Liu, X. Xu, H. An, W. Pei, and S. Zhu, Front. Comput. Sci. China **4**, 480 (2010).
[56] J. P. Perdew, K. Burke, and M. Ernzerhof, Phys. Rev. Lett. **77**, 3865 (1996).
[57] M. Methfessel and A. T. Paxton, Phys. Rev. B **40**, 3616 (1989).
[58] S. Nosé, J. Chem. Phys. **81**, 511 (1984).
[59] R. Stedman, Z. Amilius, R. Pauli, and O. Sundin, J. Phys. F: Met. Phys. **6**, 157 (1976).
[60] G. Grimvall, B. Magyari-Köpe, V. Ozoliņš, and K. A. Persson, Rev. Mod. Phys. **84**, 945 (2012).
[61] R. C. Shukla and H. Hübschle, Phys. Rev. B **40**, 1555 (1989).
[62] F. Birch, J. Geophys. Res. Solid Earth **83**, 1257 (1978).
[63] V. V. Dremov, A. A. Rykounov, F. A. Sapozhnikov, A. V. Karavaev, S. V. Yakovlev, G. V. Ionov, and M. V. Ryzhkov, J. Appl. Phys. **118**, 035901 (2015).
[64] J. P. Perdew and A. Zunger, Phys. Rev. B **23**, 5048 (1981).
[65] G. W. Stinton, S. G. MacLeod, H. Cynn, D. Errandonea, W. J. Evans, J. E. Proctor, Y. Meng, and M. I. McMahon, Phys. Rev. B **90**, 134105 (2014).
[66] J. A. Moriarty and J. D. Althoff, Phys. Rev. B **51**, 5609 (1995).
[67] S. Mehta, G. D. Price, and D. Alfè, J. Chem. Phys. **125**, 194507 (2006).
[68] H.-F. Song, H.-F. Liu, G.-C. Zhang, and Y.-H. Zhao, Chin. Phys. Lett. **26**, 066401 (2009).
[69] H.-F. Song and H.-F. Liu, Phys. Rev. B **75**, 245126 (2007).
[70] H. Liu, H. Song, Q. Zhang, G. Zhang, and Y. Zhao, Matter Radiat. Extremes **1**, 123 (2016).
[71] M. P. Desjarlais, Phys. Rev. E **88**, 062145 (2013).
[72] T. Sun, J. Xian, H. Zhang, Z. Zhang, and Y. Zhang, J. Chem. Phys. **147**, 194505 (2017).